Heliyon 9 (2023) e19877

Contents lists available at ScienceDirect

Heliyon

journal homepage: www.cell.com/heliyon

Tobramycin-loaded nanoparticles of thiolated chitosan for ocular drug delivery: Preparation, mucoadhesion and pharmacokinetic evaluation

Sadaf Javed [a], Ghulam Abbas [a], Shahid Shah [b], Akhtar Rasul [a], Muhammad Irfan [a,*], Ammara Saleem [c], Khaled M. Hosny [d], Sahar M. Bukhary [e], Awaji Y. Safhi [f], Fahad Y. Sabei [f], Mohammed A. Majrashi [g], Hala M. Alkhalidi [h], Mohammed Alissa [i], Sajid Mehmood Khan [j], Muhammad Hanif [k,**]

[a] Department of Pharmaceutics, Faculty of Pharmaceutical Sciences, Government College University Faisalabad 38000, Pakistan
[b] Department of Pharmacy Practice, Faculty of Pharmaceutical Sciences, Government College University Faisalabad 38000, Pakistan
[c] Department of Pharmacology, Faculty of Pharmaceutical Sciences, Government College University Faisalabad 38000, Pakistan
[d] Department of Pharmaceutics, Faculty of Pharmacy, King Abdulaziz University, Jeddah 21589, Saudi Arabia
[e] Department of Biological Analysis, Neuroscience unit, King Abdulaziz University, Jeddah, Saudi Arabia
[f] Department of Pharmaceutics, College of Pharmacy, Jazan University, Jazan 45142, Saudi Arabia
[g] Department of Pharmacology, College of Medicine, University of Jeddah, Jeddah 23890, Saudi Arabia
[h] Department of Clinical Pharmacy, Faculty of Pharmacy, King Abdulaziz University, Jeddah, Saudi Arabia
[i] Department of Medical Laboratory Sciences, College of Applied Medical Sciences, Prince Sattam bin Abdulaziz University, Al-Kharj 11942, Saudi Arabia
[j] Faculty of Pharmacy and Alternative Medicine, The Islamia University Bahawalpur, Pakistan
[k] Department of Pharmaceutics, Faculty of Pharmacy, Bahauddin Zakariya University Multan, Pakistan

ARTICLE INFO

Keywords:
Thiolated chitosan
nanoparticles
Mucoadhesion
Ocular irritation test
Antimicrobial activity
Pharmacokinetics
Sustainability of natural resources

ABSTRACT

The present work aimed to develop nanoparticles of tobramycin (TRM) using thiolated chitosan (TCS) in order to improve the mucoadhesion, antibacterial effect and pharmacokinetics. The nanoparticles were evaluated for their compatibility, thermal stability, particle size, zeta potential, mucoadhesion, drug release, kinetics of TRM release, corneal permeation, toxicity and ocular irritation. The thiolation of chitosan was confirmed by ^{1}H NMR and FTIR, which showed peaks at 6.6 ppm and 1230 cm^{-1}, respectively. The nanoparticles had a diameter of 73 nm, a negative zeta potential (−21 mV) and a polydispersity index of 0.15. The optimized formulation, NT8, exhibited the highest values of mucoadhesion (7.8 ± 0.541h), drug loading (87.45 ± 1.309%), entrapment efficiency (92.34 ± 2.671%), TRM release (>90%) and corneal permeation (85.56%). The release pattern of TRM from the developed formulations was fickian diffusion. TRM-loaded nanoparticles showed good antibacterial activity against *Pseudomonas aeruginosa*. The optimized formulation NT8 (0.1% TRM) greatly increased the $AUC_{(0-\infty)}$ (1.5-fold) while significantly

* Corresponding author.
** Corresponding author.
E-mail addresses: sadaf.rajpoot11@gmail.com (S. Javed), ghulamabbas@gcuf.edu.pk (G. Abbas), shahid.shah@gcuf.edu.pk (S. Shah), akhtar.rasul@gcuf.edu.pk (A. Rasul), manipharma@yahoo.co.uk (M. Irfan), ammarasaleem@gcuf.edu.pk (A. Saleem), kmhomar@kau.edu.sa (K.M. Hosny), bukharysahar@gmail.com (S.M. Bukhary), asafhi@jazanu.edu.sa (A.Y. Safhi), fsabei@jazanu.edu.sa (F.Y. Sabei), mamajrashi@uj.edu.sa (M.A. Majrashi), halkhaldi@kau.edu.sa (H.M. Alkhalidi), m.alissa@psau.edu.sa (M. Alissa), smk.rao83@gmail.com (S.M. Khan), muhammad.hanif@bzu.edu.pk (M. Hanif).

https://doi.org/10.1016/j.heliyon.2023.e19877
Received 27 May 2023; Received in revised form 4 September 2023; Accepted 4 September 2023
Available online 7 September 2023

reducing the clearance (5-fold) compared to 0.3% TRM. Pharmacokinetic parameters indicated improved ocular retention and bioavailability of TRM loaded nanoparticles. Our study demonstrated that the TRM-loaded nanoparticles had improved mucoadhesion and pharmacokinetics and a suitable candidate for effective treatment of ocular bacterial infections.

1. Introduction

The eye is often colonized by the microbiota. Commonly, the degree of eye stiffness and the protection of the eye from infections depend on the constant bathing of the eye with tears, which contain antibacterial compounds [1]. If inflammation and scarring of the eye occur, their immediate control is required. The main causes of ophthalmic infection are bacteria that are present in the outside environment or that enter the eye because of the prolonged use of contact lenses [2]. Infections can be due to one or several bacteria and often spread to nearby tissues. Infection due to the continuous interaction of the eye with the external environment, which is the main source of infection, occurs even though the ophthalmic surface has a fully established immune system [3]. The bacterial ophthalmic infections include conjunctivitis, keratitis, blepharitis, orbital cellulitis, and dacryocystitis [4].

Ophthalmic drug delivery is a great challenge for scientists due to the eye's unique structure and physiology. Eye conditions are treated by applying drugs topically in the form of solutions, suspensions, and ointments [5]. Because of the various structural and pathophysiological obstacles typically found in the eye, these dosage forms suffer from problems of reduced ophthalmic bioavailability [6]. Various conventional and novel delivery systems, such as ointments, emulsions, suspensions, the aqueous gel of nanomicelles, liposomes, nanoparticles, implants, dendrimers, nanosuspensions, contact lenses, in situ heat-sensitive gels, and microneedles, have been developed for ophthalmic diseases [7]. Recent delivery systems include microemulsion, nanosuspensions, nanoparticles, liposomes, niosomes, dendrimers, and cyclodextrins [8].

The low ophthalmic bioavailability (<10%) of conventional formulations has forced scientists to develop new formulations that can deliver drugs to ophthalmic tissues at a precise rate [9]. Advanced nanoparticulate systems aimed to raise the bioavailability of drugs at the ophthalmic surface. In ophthalmic drug delivery, particles of a suitable size reduced ocular irritation [10]. For ophthalmic tissues, drugs need to have a suitable bioavailability and compatibility. The ideal ophthalmic form of delivery of a drug would be an eye drop that did not cause blurred vision or require more than two administrations per day [8]. One important feature of the formulation is its mucoahesiveness (i.e., its interaction with the mucin present on the eye). The development of eye drops and pharmaceutical approaches based on nanotechnology that use chitosan mucoadhesive polymers is of interest for the efficient treatment of ophthalmic diseases [11]. A chitosan nanoparticle is a drug carrier that provides the controlled/slow release of a drug, which improves the drug's solubility, stability, and efficacy and decreases the drug's toxicity. Because of the nanoparticles small size, it traverses biological obstacles and delivers drugs to the desired site with improved efficacy [12]. Nanoparticles of a modified polymer (i.e., the thiolation of chitosan) provided improved mucoadhesion and enhanced retention of the drug in the eye [13].

Thiolated chitosan (TCS) has various benefits over other types of modified polymers, including their antibacterial activity. It inhibits the growth of bacteria, has good mucoadhesion, and slows the release of a drug. In one study, TCS enhanced the retention of a drug in the ophthalmic region and had little toxicity [14]. TCS is basically created by attaching chemicals with thiol functions to the main amino groups of chitosan. Thiolated polymers have shown enhanced permeation, which was due to the interaction of positive and negative charges between the thiolated polymers and the tight junctions and allowed for the transport of a drug by opening the junctions [15]. The purpose of the study was to develop a TCS that would enhance the mucoadhesion and permeation of TRM. The TCS was evaluated by hydrogen^{-1} nuclear magnetic resonance (^{1}H NMR) and Fourier-transform infrared spectroscopy (FTIR), and the developed nanoparticles were evaluated for their zeta potential, size, ocular irritation, antibacterial activity, and thermal properties. The *in vivo* ocular retention and pharmacokinetics of TRM were evaluated in sheep.

Ethics approval

The animal study protocol was approved by the Institutional Review Board (or Ethics Committee) of Government College University Faisalabad, Pakistan (protocol code 002278 and 06-22-2022).

2. Materials and methods

2.1. Materials

Chitosan (CS) and 3-mercaptopropionic acid (3MPA) were purchased from Sigma Aldrich GmbH, Darmstadt, Germany. Potassium dihydrogen phosphate, ethanol, methanol, acetonitrile, 1-ethyl-3-(3-dimethylaminopropyl) carbodiimide (EDC), and N-hydroxysuccinimide (NHS) were purchased from Merck, Darmstadt, Germany. Dimethylformamide, hydrochloric acid (HCl), and sodium hydroxide (NaOH) were acquired from BDH, London, UK. Tobramycin (TRM) was obtained as a gift sample from Vega Pharmaceuticals, Lahore, Pakistan.

2.2. Thiolation and characterization of CS

The thiolation of CS was done by a slight modification of the method reported by Esquivel et al., in 2015 [15]. It underwent two reaction processes. First, a 100-mL three-necked flask was charged with 2 mL of dimethylformamide before being filled with 0.104 mmol of EDC, 0.208 mmol of 3MPA, and 0.104 mmol of NHS. The mixture was held overnight at room temperature while constantly being stirred. O-acylisourea was produced in the first stage of the reaction, and the sulfo-NHS ester that reacts with the intermediate amines was also activated. The pH was then brought down to 5.5 with 1 M NaOH before 20 mL of a 5% CS solution was created. We used a syringe to add the intermediate solution one drop at a time. The final mixture was agitated for 12 h at room temperature. The crude combination was dialyzed (Cellu/Sep MWCO for 5000 membrane dialysis) with 0.01 M HCl and deionized water to remove unbound 3MPA and isolate the thiolated chitosan (TCS). Centrifugation at 5000 rpm was used to separate the polymer from the product after it had been precipitated with 50 mL of ethanol (in triplicate; Allegra X-22 centrifuge, F1010 rotor). To ensure that the CS was pure, it was freeze-dried and then examined using spectroscopic methods. The thiolation of CS was confirmed by ^{1}H NMR and FTIR.

2.3. Preparation of nanoparticles

One gram of TCS was dissolved in a 1% (w/v) acetic acid solution and sonicated until a clear solution was obtained. The TCS solution was diluted with deionized water to make concentrations of 0.10%, 0.20%, 0.50%, and 0.80%. The TCS solutions were then combined with the same volume of a sodium tripolyphosphate (TPP) solution, and the TCS-TPP nanoparticles were formed by the TPP-initiated ionic gelation process. Then, a TPP solution was made by dissolving 0.7 mg of TPP in 100 mL of deionized water. The weight ratios of TCS to TPP were synthesized at 1:1, 2:1, 3:1, 4:1, 5:1, 6:1, 7:1, 8:1, and 9:1. Centrifugation at 6000 rpm for 20 min was done to obtain the nanoparticles [16].

2.4. Loading of TRM

Amounts of 0.01 mg of nanoparticles and 0.01 mg of TRM were weighed, dispersed in 4 mL of deionized water, and stirred for 24 h. After stirring, centrifugation was done at 6000 rpm for 20 min. The prepared formulations and their compositions are shown in Table 1.

2.5. Entrapment efficiency and loading of TRM

An amount of 2 mL was taken from the drug-loaded solution with an Eppendorf tube and centrifuged at 6000 rpm for 20 min to form a supernatant layer containing drug. This supernatant layer was filtered using cellulose acetate membrane filter having pore size 0.45 μm and its absorbance was measured after dilution. The same procedure was repeated for the other formulations. The entrapment efficiency and loading of TRM was calculated using equations (1) and (2) respectively.

$$Entrapment\ efficiency = \frac{Total\ amount\ of\ drug - Amount\ of\ drug\ in\ solution}{Total\ amount\ of\ drug\ used} \times 100 \quad (1)$$

$$Drug\ loading\ (\%) = \frac{Total\ amount\ of\ drug - Amount\ of\ drug\ in\ solution}{Total\ amount\ of\ formulation\ used} \times 100 \quad (2)$$

2.6. Characterization

2.6.1. Particle size analysis and zeta potential

Photon correlation spectroscopy with a Zeta-sizer 3000 was used to demonstrate the distribution size of the nanoparticles and their

Table 1
Composition of prepared nanoparticles.

Formulation	Ratio	
	TCS	TPP
NT1	10	10
NT2	20	10
NT3	30	10
NT4	40	10
NT5	50	10
NT6	60	10
NT7	70	10
NT8	80	10
NT9	90	10

TCS is thiolated chitosan and TPP is tripolyphosphate.

zeta potential (Malvern Instruments, Inc., Malvern, Worcester shire, UK). At a temperature of 25 °C and a scattering angle of 90°, a size distribution analysis was conducted. The samples were properly diluted with ultrapure water, and the zeta potential was determined using a disposable zeta cuvette and electrophoretic light scattering. The results were displayed as the mean plus or minus the standard deviation (SD). The particle size of the optimized formulation was also measured after 7, 14 and 30 days after preparation.

2.6.2. Differential scanning calorimetry (DSC) and thermogravimetric analysis (TGA)

The TRM, CS, TCS, NT8 blank and TRM-loaded nanoparticles were evaluated using a DSC-TGA analyzer (PerkinElmer, 60A, Germany DSC/TGA calorimeter) for thermal stability studies.

2.6.3. Fourier-transform infrared spectroscopy (FTIR) and x-ray diffusion (XRD) analysis

The TRM, CS, TCS, NT8 blank and TRM-loaded nanoparticles were evaluated for compatibility and amorphous nature/crystallinity using FTIR (Bruker Alpha, Germany) and XRD using X-ray diffractometer (D/max-2500pc, Rigaku. Co, Japan).

2.7. TRM release and kinetics

In vitro release of TRM from nanoparticles was studied using 30 mL of phosphate buffered solution at pH 7.4. The nanoparticles were put in a dialysis bag (molecular weight cut-off 14,000) with 5 mL of dissolution media. Thirty milliliters of buffer was added to the beaker. The beaker was placed in a water bath (Daihan Scientific, Wonju, Kang won-do, South Korea), which was continuously stirred at 100 rpm while a temperature of 37 °C was maintained. At different time intervals (0.5, 1, 2, 3, 4, 5, 6, 7 and 8 h), 3 mL of the dissolution medium was removed and 3 mL of the fresh dissolution medium was added to maintain sink conditions. The cumulative TRM release into the dissolving liquid was calculated using HPLC (Shimadzu LC-10AT and LC-10AT VP pumps, a manually operated 20 μL sample loop, and a UV–Visible detector (SPD 10A VP) make up the HPLC system).To determine the specific release pattern of the drug, dissolution statistics were applied by a kinetic model, that is, the zero-order model, first-order model, Higuchi model, Hixson–Crowell model, or Korsmeyer–Peppas model [17,18].

2.8. Permeation study

Within an hour of the animal being sacrificed, fresh sheep's eyes were obtained from a nearby butcher shop. The entire eye was dissected, and the cornea plus a 5-mm-broad sclera attached was tested for permeation in simulated tear fluid (phosphate buffered solution at pH 7.4) at 37 °C using a vertically oriented Franz diffusion cell. The donor compartment was directly in front of the dorsal side of the cornea. At regular intervals, samples were taken from the receptor compartment and passed through a 0.45-μm membrane filter. Using a UV-VIS spectrophotometer, absorbance values were recorded at 235 nm (JASCO V-630 spectrophotometer, JASCO International, Tokyo, Japan) [19].

2.9. Cell viability assay

The MTT (3-(4,5-dimethylthiazol-2-yl)-2,5-diphenyl-2H-tetrazolium bromide) assay was applied to the ARPE-19 cell line to determine the cellular toxicity of the CS, TCS, NT8 blank and TRM-loaded nanoparticles. ARPE-19 is a human retinal pigment epithelial cell line derived from the normal eyes of a 19-year-old male who died from head trauma in a motor vehicle accident and is the ideal model for analyzing the cytotoxicity of TRM-loaded nanoparticles. The cells were cultivated on Dulbecco's Modified Eagle Medium with 10% fetal bovine serum (FBS) in 96-well plates. Cells were cultured for 6 and 24 h in FBS-free growth medium that contained 0.5% dispersions of various samples after confluence. After incubation, the cells were washed with phosphate buffered saline (1X PBS). MTT solutions of 500 μL in FBS-free medium were added after that (0.5 mg/mL), and the cells were once more incubated for 1 h. DMSO 500 μL was added to each well after the supernatant was drained in order to solubilize the converted dye.

The absorbance at 570 nm was measured using a SpectraMax M5 microplate reader (Molecular Devices, Sunnyvale, CA, USA). The cell viability rates (VR) were calculated according to Equation (3);

$$VR = \frac{A - A_0}{A_S - A_0} \times 100\% \tag{3}$$

Where A is the absorbance of the experimental group, A_S is the absorbance of the control group and A_0 is the absorbance of the blank group.

2.10. Antibacterial analysis

The most frequent bacteria associated with ocular infections are *Staphylococcus aureus, Streptococcus pneumoniae, Bacillus, Pseudomonas aeruginosa, Enterobacteriaceae* and *Haemophilus influenza*. Ampicillin, chloramphenicol, neomycin, gentamycin, ciprofloxacin and tobramycin are used for the management of bacterial infections. Due to the secretion of proteases, *Pseudomonas aeruginosa* is an opportunistic bacterium that frequently causes ocular infections such as bacterial keratitis, which damages and perforates the cornea. *P. aeruginosa* related ocular infections were reported in the majority of clinical and animal research [20,21]. *P. aeruginosa* released enzymes and toxins that damaged the extracellular matrix of the cornea as well as its cellular components, activating and releasing

enzymes that break down the cornea. We chose *P. aeruginosa* as the test organism for the antibacterial activity of the TRM-loaded nanoparticles that were created in the current investigation. The antibacterial efficacy of the TRM-loaded nanoparticles was assessed using the agar well diffusion method, and the medium was nutrient agar. Using the streak method, *Pseudomonas aeruginosa* was used to infect the agar plate. With the aid of a sterile cork borer, a hole of 6–8 mm in diameter was made, and each well received 20 μL of the optimal formulation NT8 (TRM-loaded nanoparticles), NT8 blank, TRM pure drug, or control (i.e., no treatment) and was incubated for 24 h.

2.11. Ophthalmic irritation study

The Draize test of ocular irritation of the TRM-loaded nanoparticles was conducted on 12 albino rats (6 for the control and 6 for the NT8-treated group). After every 30 min for 6 h, 20 μL of the TRM-loaded nanoparticles (NT8-treated group) was inserted into the cornea of the right eye. The TRM was administered to the left eye, serving as the control. The ocular tissue was assessed at the end of the 8 h treatments. A scale was used to assess the conjunctival edema, discharge, and conjunction. The corneal capacity and irritation scales ranged from 0 to 4 [22].

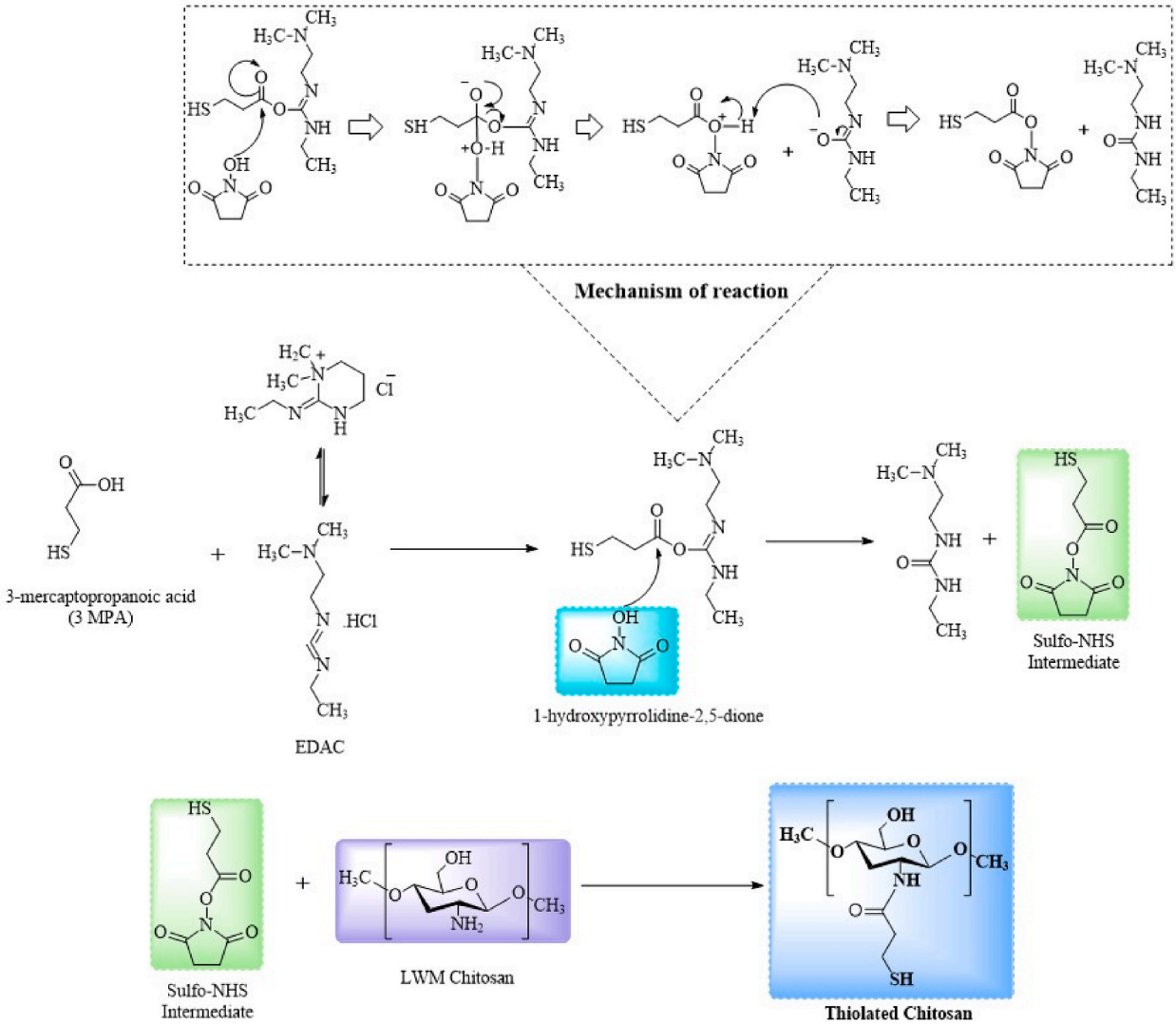

Fig. 1. Schematic representations of the formation of thiolated chitosan. The arrow drawing presented the nucleophilic attack of the OH group of 1-hydroxypyrrolidine-2,5-dione on the carbonyl ester carbon of the adduct formed by reacting 3MPA with EDAC, leading to the urea derivative and the desired sulfo-NHS intermediate. Sulfo-NHS intermediate react with LMW chitosan to form thiolated chitosan.

2.12. Mucoadhesive evaluation

Mucoadhesion was evaluated on freshly cut sheep eyelids. The CS, TCS, and NT8 TRM-loaded formulation were instilled on the eyelid's mucosal surface. It was adhered to the bottom of a beaker. Bicarbonate Ringer solution at pH 7.4 was added to the beaker and it was agitated at a rate of 150 rpm at 33 °C. The detachment time of the applied formulations was noted [23].

2.13. HPLC method for determination of TRM

A HPLC technique was created and approved for TRM quantification. The investigation included the selection of an appropriate mobile phase as well as flow rate, detection wavelength, and mobile phase pH optimisation. An isocratic mobile phase composed of 45:55 volumetric ratio of methanol and potassium dihydrogen phosphate pH 6.8. The chromatography was carried out at 25 °C and the detection wavelength set at 235 nm. TRM were eluted isocratically at a constant flow rate of 1.25 mL/min using a C_{18} column. Following ICH criteria, the approach was approved, and interday and intraday precision were calculated as well as correlation coefficients (R^2) for TRM obtained in the linearity study. All of the HPLC processes validating parameters were calculated together with drug recovery, LOD and LOQ determination, and RSD. Shimadzu LC-10AT and LC-10AT VP pumps, a manually operated 20 μL sample

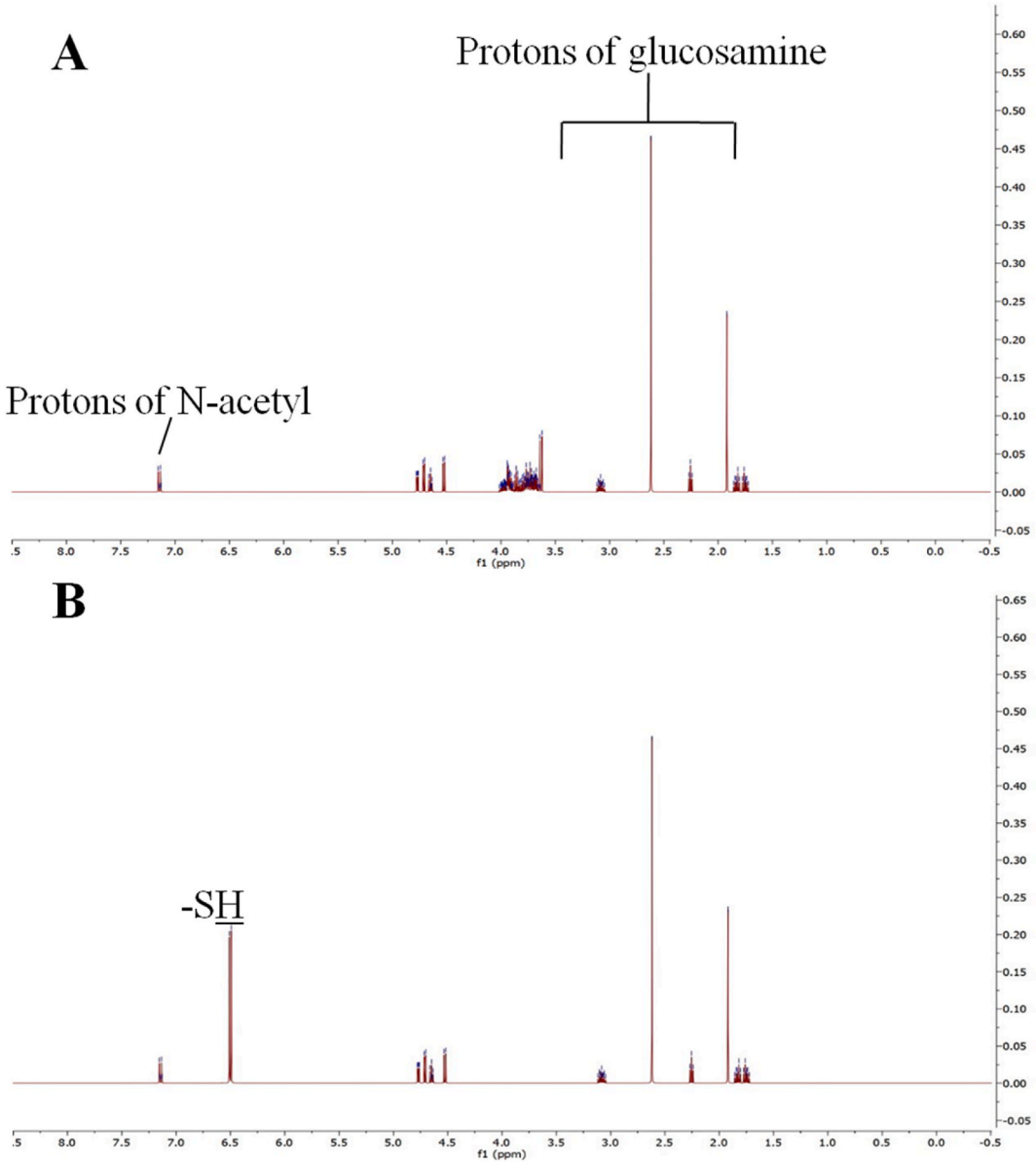

Fig. 2. NMR of CS (A) and TCS (B) shows a thiol group peak of 6.6 ppm.

loop, and a UV–Visible detector (SPD 10A VP) make up the HPLC system. Software for Shimadzu class-VP version 6.12 SP1 integrated the output signal. The mobile phase was passed through column C_{18} (250 mm × 4.6 mm, 5 μm particle size) after being filtered using a 0.22 μm membrane filter.

2.14. In vivo ocular retention and pharmacokinetic study

Pharmacokinetic parameters following the ocular administration of TRM at dose strengths of 0.3% w/v as the TRM-loaded NT8 formulation and 0.1% w/v TRM were determined. In the course of the experiment, restraining cages were used to hold the sheep while allowing for free eye and head movement and free food intake. Using a micropipette, 20 μL of each formulation was administered into the lower conjunctival sac of the left cornea, avoiding any possible contact with the eye that could irritate the surface of the cornea. At intervals of 5, 15, 30, 45, 60, 90, 120, 150, 180, 210, and 240 min following instillation, 10 μL of lachrymal fluid was drawn out from the site of administration using a calibrated glass capillary. Samples were kept in microcentrifuge tubes at −20 °C prior to analysis. The highly sensitive high-performance liquid chromatography (HPLC) method permitted use of only 20 μL of the lacrimal sample to determine the amount of TRM.

2.15. Statistical analysis

The statistical discrepancy between treatments was evaluated using the analysis of variance (ANOVA) test. The examination comprised comparisons among groups using the Dunnett's test, as well as the calculation of means, standard errors, and other metrics. The confidence interval was set at 95%, and the significance threshold was a *p*-value of.05 or less.

3. Results and discussion

3.1. Preparation and characterization of thiolated chitosan

Fig. 1 shows the interaction of chitosan with 3MPA in the presence of EDC and NHS coupling agents. Nine formulations of nanoparticles were prepared successfully. The CS that was thiolated had free thiol levels of between 0.06 and 0.17 mmoL/mg. It produced formulations NT1 to NT9 of nanoparticles that had free thiol levels of 0.04–0.16 mmoL/mg. The protons of the glucosamine unit of CS found in the ^{1}H NMR spectra showed peaks of 1.9–3.7, and the methyl protons of the N-acetyl group that were found had a peak of 7.2, as shown in Fig. 2A [24]. The new peak at 6.6 showed the commencement of the thiol functional group in TCS (Fig. 2B).

3.2. Entrapment efficiency and loading of TRM

The entrapment efficiency of the NT1 to NT9 formulations ranged from 52.32 ± 1.213% to 92.34 ± 2.671%, while the percentage range of TRM loaded in formulations NT1 to NT9 was 43.43 ± 1.13% to 87.45 ± 1.309%. NT8 exhibited the highest levels of TRM loading and entrapment efficiency, as shown in Table 2. Increasing the drug loading capacity of the composite nanoparticles enhances the encapsulation efficiency to reach 92% at a loading capacity of 87%. When the polymer concentration was raised to 80%, the drug loading increased. The medication loading was lowered as polymer concentration rose above 80%. The amount of TPP remained at 10% even though the drug loading in NT9 was reduced as the TCS concentration rose. The decrease in TRM loading was due to the concentration of crosslinker in nanoparticles. The drug nano-carrier's effectiveness can be improved, resulting in a more significant therapeutic benefit and fewer side effects. The created nanoparticles have the advantage of improved drug encapsulation, according to the study's effectiveness in entrapment values, showing the potential to maximise the medical benefits of TRM and produce improved long-lasting drug release.

3.3. Characterization of nanoparticles

3.3.1. Particle size analysis and zeta potential

Fig. 3A displays the particle size distribution of the NT8 formulation. The polydispersity index (PDI) of formulations NT1 to NT3

Table 2
Loading of TRM in and entrapment efficiency of formulations NT1 to NT9.

Formulation	Entrapment Efficiency (%)	TRM Loading (%)
NT1	52.32 ± 1.213	43.43 ± 1.13
NT2	56.56 ± 1.215	48.76 ± 1.125
NT3	59.45 ± 1.314	55.34 ± 1.149
NT4	51.39 ± 1.412	45.56 ± 1.251
NT5	61.45 ± 1.514	58.76 ± 1.259
NT6	69.56 ± 1.912	63.19 ± 1.271
NT7	65.89 ± 2.325	61.67 ± 1.291
NT8	92.34 ± 2.671	87.45 ± 1.309
NT9	87.49 ± 2.421	82.45 ± 1.301

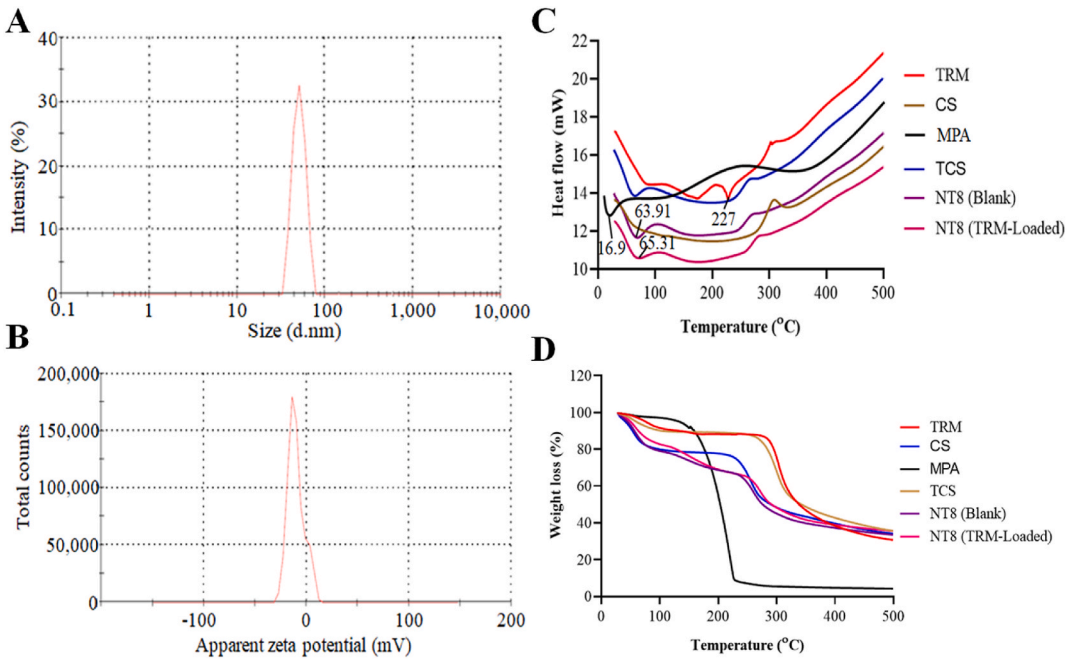

Fig. 3. Particle size distribution (A) and zeta potential (B) of NT8 nanoparticle formulation. Differential scanning calorimetry (DSC) (C) and thermogravimetric analysis (TGA) (D) of TRM, CS, 3MPA, TCS, NT8 blank, and NT8 TRM-loaded.

was more than 0.4, as shown in Table 3, while in formulations NT4 to NT9 it was less than 0.4; this indicated the uniform size of the nanoparticles [14]. The average particle diameter in the NT8 formulation was 73 nm; particles having a large size have more difficulty in becoming diffused through mucus pores [24]. The zeta potential is important for formulation stability as it prevents aggregation. Table 3 shows that formulations NT1 to NT9 had zeta potentials of −10 to −21; NT8 was the most stable of the formulations (Fig. 3B). A zeta potential of −21 mV indicated sufficient stability; a negative surface charge revealed that repulsive forces among particles were dominant and would resist aggregation. Therefore, it is anticipated that the nanoparticles' negative charge will considerably improve their interaction with the mucosal membrane of the eye. A negative zeta potential value also produces a repelling force between the nanoparticles, which can help to stabilize them [25]. The particle size of the NT8 formulation was 79 nm, 86 nm, and 99 nm after 7, 14 and 30 days storage. Following the 30-day storage, there were no significant changes in particle size.

3.3.2. Differential scanning calorimetry (DSC)

In Fig. 3C, the DSC of TRM showed an endothermic peak at 227 °C as it consented to the stable anhydrous form [26]. 3MPA showed a sharp peak at 16.9 °C that was related to the melting point [27]. Because TCS has a side chain that is easily broken due to thiolation, an exothermic peak was seen at 270 °C. The deterioration of the amine unit caused the CS to exhibit an exothermic peak at 305 °C [28]. The NT8 blank showed an endothermic peak at 63.91 °C, and the NT8 TRM-loaded nanoparticles showed an endothermic peak at 65.31 °C. The acquired results focused on the DSC thermograms of the TRM-loaded nanoparticles and revealed that no endothermic peak corresponding to the TRM was observed in any of the cases, revealing that the TRM was likely spread in an amorphous condition.

3.3.3. Thermogravimetric analysis (TGA)

TRM showed a weight loss at 32 °C and 258 °C due to the hygroscopic nature of the formulations; this could be attributed to the loss of water and volatile components from the samples as a result of a dehydration reaction [29]. In Fig. 3D, the TGA of CS shows a weight

Table 3
Particle size, PDI, and zeta potential values of developed nanoparticles.

Formulation	Size of Particles (nm)	PDI	Zeta Potential (mV)
NT1	189 ± 3.129	0.458 ± 0.014	−12 ± 1.2
NT2	156 ± 3.098	0.401 ± 0.015	−15 ± 1.3
NT3	143 ± 2.432	0.482 ± 0.021	−16 ± 1.4
NT4	139 ± 1.985	0.308 ± 0.010	−12 ± 1.1
NT5	134 ± 1.023	0.213 ± 0.002	−11 ± 1.0
NT6	112 ± 1.002	0.398 ± 0.013	−10 ± 1.3
NT7	106 ± 1.560	0.178 ± 0.031	−17 ± 1.4
NT8	73 ± 1.109	0.156 ± 0.001	−21 ± 1.1
NT9	137 ± 2.103	0.304 ± 0.024	−18 ± 1.3

loss at 32 °C–191 °C. The decomposition took place in two steps. First, it was related to water evaporation, and second, it was related to the degradation of the main chain of the CS [30]. TCS began a weight loss at 235 °C and ended it at 342 °C. The degradation took place in two steps. First, it was due to water absorbed or bonded to the polymer structure, and second, it was due to the degradation of the amide bridge [31]. 3MPA showed a weight loss beginning at 34 °C and ending at 235 °C owing to the degradation of the carboxylic and thiol groups. 3MPA is a volatile compound and quickly loses mass [32,33]. The NT8 blank nanoparticles showed a weight loss at 30 °C–216 °C owing to the decomposition of the encapsulated 3MPA in the chitosan nanoparticles; the increased thermal stability reduced the rate of weight loss [32]. The TRM-loaded NT8 formulation had weight loss at 31 °C–271 °C, and this indicated that the formulation had thermal stability.

3.3.4. *Fourier-transform infrared spectroscopy (FTIR)*

The FTIR spectra of TRM and other used excipients are shown in Fig. 4A. TRM showed absorption peaks at 1000 cm^{-1}, 1345 cm^{-1}, and 1583 cm^{-1} related to NH bending. Another broad band was seen at approximately 2970 $cm^{-1}$and was related to the OH and NH groups [34]. FTIR spectra of CS showed absorption peaks of the –NH amine stretching vibration at 3410 cm^{-1}, an absorption band of the C–H group at 2924 cm^{-1}, C═O stretching at 1710 cm^{-1}, and a C–O stretching vibration at 1088 cm^{-1} [35]. Fig. 5 shows that CS that had been thiolated had peaks of the thiol group (C-SH) at 1230 cm^{-1} and 1629 cm^{-1} (amide I band), and this was evidence that the CS had been thiolated [36]. 3MPA showed absorption peaks at 1710 cm^{-1}owing to –N-C-S stretching, 1410 cm^{-1} due to –C-H stretching, and 995 cm^{-1} due to the stretching vibration of –N-C [27]. The drug-loaded nanoparticle formulation (NT8) showed many peaks as a result of TCS. Many peaks appeared and disappeared, and this verified that interactions were occurring among TRM, TCS, and 3MPA in the nanoparticles. Absorption peaks at 1000 cm^{-1}, 1629 cm^{-1}, and 1583 cm^{-1} were observed [37].

3.3.5. *X-ray diffraction (XRD) analysis*

TRM peaks indicated a crystalline form, and 3MPA was associated with low-intensity peaks and an amorphous nature, as shown in Fig. 4B. XRD of CS revealed a prominent peak at 20(θ) and intensity at 250, verifying a crystalline nature; in the case of TCS, the intensities of the sharp peaks were reduced to 150 due to thiol conjugation [38]. The NT8 blank nanoparticles had a less pronounced crystalline nature because of cross linking among the reactive forms of the functional group in TCS and TPP caused by 3MPA via coupling agents [35]. The NT8 TRM-loaded nanoparticles had no diffraction peaks; this indicated a uniform distribution of TRM and an amorphous nature. No TRM distinctive peaks were seen in the resultant diffractogram for the TRM-loaded nanoparticles, proving that the production procedure yielded nanoparticles with TRM that was still amorphous.

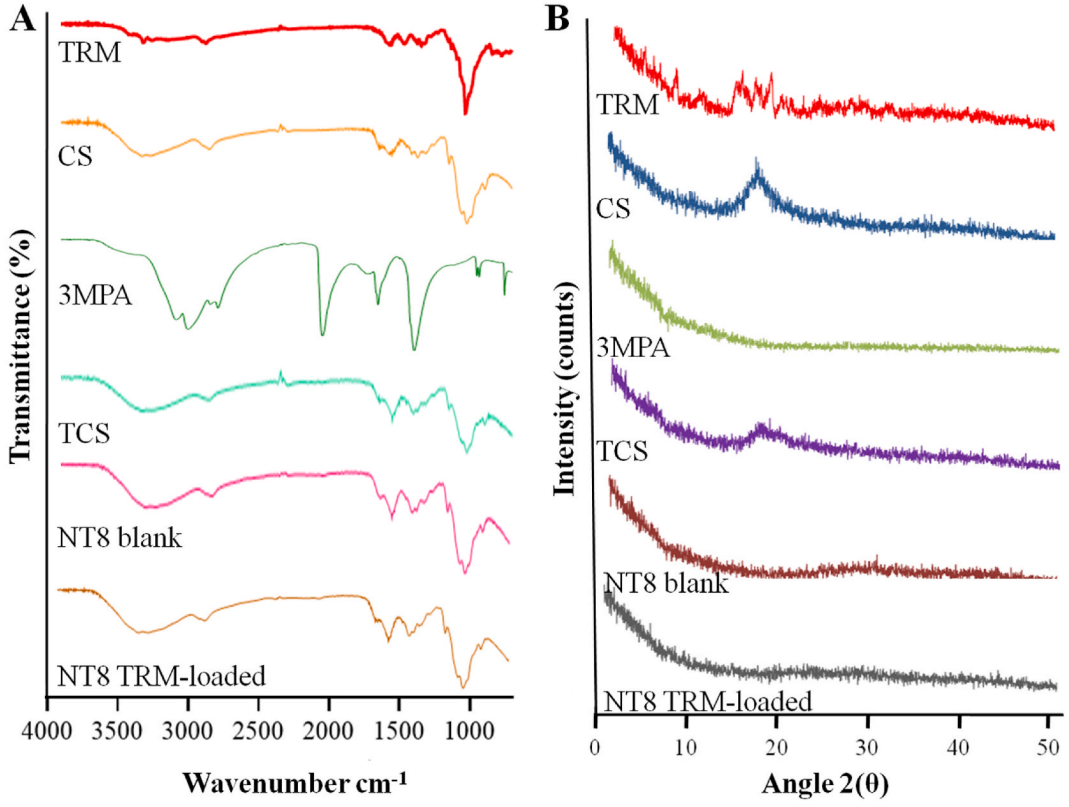

Fig. 4. FTIR (A) and XRD (B) of TRM, CS, 3MPA, TCS, NT8 blank, and NT8 TRM-loaded nanoparticles.

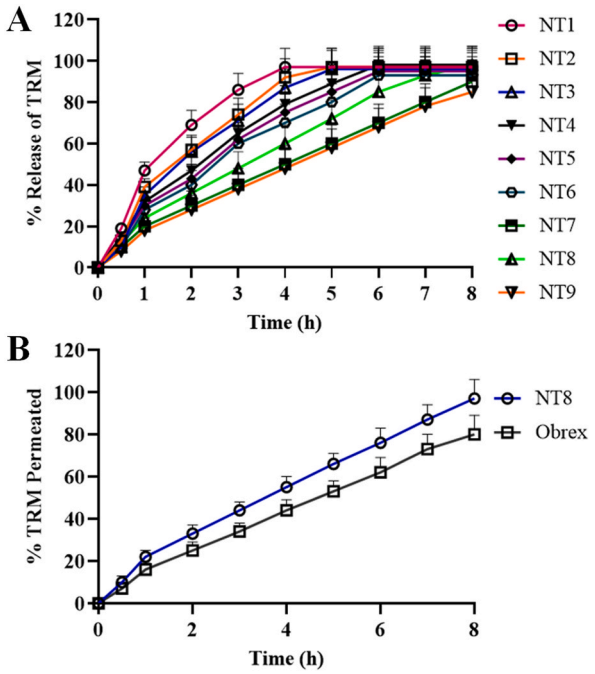

Fig. 5. TRM release from developed formulations (A) and permeation study using sheep cornea (B) in phosphate buffered solution at pH 7.4.

3.4. In vitro release and kinetics of TRM

The composition of nanoparticles, the ratio of drug and polymer, the physical and chemical interactions between the components, and the preparation techniques all had an impact on how efficiently drugs were released from carriers. The release of TRM from the NTI to NT9 formulations is shown in Fig. 5A. In the NT1, NT2, and NT3 formulations, a maximum drug release of over 90.19% occurred for up to 4 h because these formulations contained 10%, 20%, or 30% TCS, respectively. The 90.56% TRM release from the NT4, NT5, and NT6 formulations was seen in 6 h; they contained greater concentrations of TCS (i.e., 40%. 50%, or 60%, respectively) compared with NT1, NT2, and NT3. Because of the greater amount of TCS retardant polymer, which sustained the release of TRM from the produced nanoparticles, the NT7, NT8, and NT9 formulations had the maximal TRM release of over 90.34% in 8 h. The increased concentration of TCS in the developed formulations had a retardant effect. The NT8 and NT9 formulations were chosen because they had drug release times that lasted for up to 8 h. TRM and TPP had opposite charges that interfered with drug release; thus, when the concentration of TCS rose, the sustained release of TRM occurred. That is why the NT8 and NT9 formulations showed sustained release effects [39]. For the TRM release, the obtained *p*-value was less than 0.001 indicating the significance of the results. In the zero-order model, the R-squared value ranged from 0.962 to 0.999, while in the first-order model, the R-squared value ranged from 0.896 to 0.953. Because the R-squared value was close to 1, our formulation followed the zero-order release pattern, as shown in Table 4. It would be ideal to create nanoparticles that could deliver a medicine in a sustained or controlled manner with a low-dose frequency. A consistent drug release rate (i.e., zero-order drug release profile) was widely employed for this purpose. In the Higuchi model, the R-squared value ranged from 0.996 to 0.999, indicating that the mechanism of release of TRM from the developed nanoparticles was diffusion, and in the Hixson–Crowell model, the R-squared value ranged from 0.991 to 0.998. In the Korsmeyer–Peppas model, the R-squared value ranged from 0.961 to 0.999 and the value of *n* was 0.5 or less, as shown in Table 4. This indicated that the release

Table 4
Values of release kinetic models for different formulations.

Formulation	Zero-order Model	First-order Model	Higuchi Model	Hixson–Crowell Model	Korsmeyer–Peppas Model	
	R^2	R^2	R^2	R^2	R^2	N
NT1	0.994	0.896	0.996	0.991	0.966	0.47
NT2	0.962	0.843	0.997	0.993	0.961	0.46
NT3	0.983	0.675	0.997	0.990	0.987	0.45
NT4	0.991	0.890	0.996	0.989	0.994	0.34
NT5	0.992	0.931	0.996	0.967	0.991	0.29
NT6	0.987	0.903	0.998	0.996	0.989	0.37
NT7	0.996	0.953	0.998	0.990	0.998	0.31
NT8	0.999	0.950	0.999	0.998	0.999	0.23
NT9	0.990	0.929	0.997	0.991	0.993	0.39

pattern of TRM from the developed formulations was fickian diffusion. The nanoparticles followed zero-order release kinetics. Fickian diffusion was noticed because the value of *n* in the Korsmeyer–Peppas model was less than 0.45.

3.5. Permeation study

The permeation data showed that the TRM-loaded nanoparticles (NT8) had enhanced permeation because they were loaded with TCS. As a result of possible additional interactions with the mucosal surface brought about by the presence of disulfide with the cysteine residue of mucin, formulation NT8 not only demonstrated improved mucosal adhesion but also a higher permeation enhancer effect, extending the residential time in the eye following topical instillation [39]. NT8 and Obrex, a commercially available eye drop, had a 98.56% and 79.12% permeation of TRM, respectively, as shown in Fig. 5B. The improved permeation of TRM with the NT8 formulation may have been due to increased mucoadhesion and retention in the eye. The obtained *p*-value was 0.01 and for the permeation study, indicating that the results were statistically significant.

3.6. Cell viability assay

Determining the cytotoxicity of a formulation is one of the most essential steps in pre-clinical research on pharmaceuticals. We evaluated the ARPE-19 cell culture's viability after it was exposed to the NT8 blank and NT8 TRM-loaded nanoparticles. Findings demonstrated that the quantity of the TRM-loaded nanoparticles utilized in the study's culture medium had no effect on the survivability of these cells, and the graph showed that after 24 h of incubation, more than 80% of the cells remained viable (Fig. 6A). Under the microscope, there was no evidence of a change in cell morphology. Control (Ctrl) group is the positive group in which only medium was used (untreated cells).

3.7. Antibacterial activity

Fig. 6B and C shows that the zone of inhibition of the NT8 TRM-loaded formulation was slightly different than that of the NT8 blank and the TRM formulations. The TRM-loaded nanoparticles showed comparable antibacterial activity to the NT8 blank and TRM, against *P. aeruginosa,* observed from the zone of inhibition. The zone of inhibition of the pure drug TRM was 31 ± 0.5 mm, while that of the NT8 TRM-loaded formulation was 34.5 ± 0.4 mm ($p < 0.001$). This may have been due to the sustained release pattern of TRM

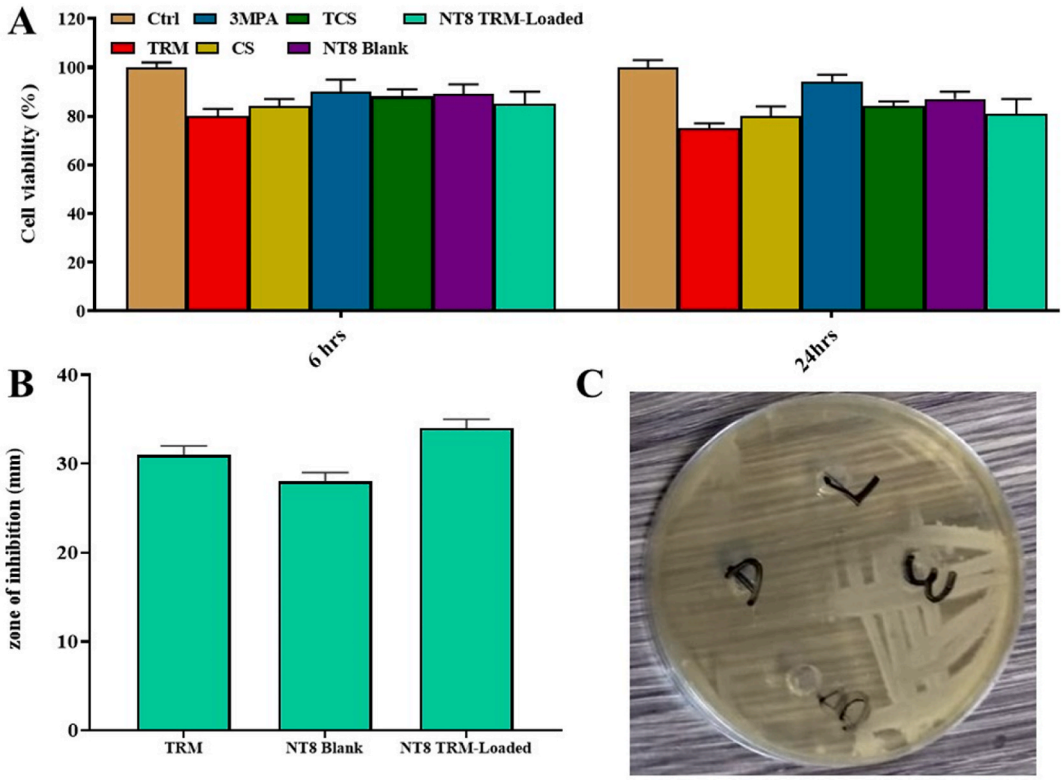

Fig. 6. Cytotoxicity and antibacterial activity of pure TRM, CS, TCS, 3MPA, NT8 blank, NT8 TRM-loaded nanoparticles, and control (A). Zone of inhibition of the TRM, NT8 blank, and NT8 TRM-loaded nanoparticles (B and C). In C, the letters D, L, B, and E represent the pure TRM, NT8 TRM-loaded nanoparticles, NT8 blank, and control, respectively.

from the NT8 formulation [40].

3.8. Ophthalmic irritation study

The cornea, conjunctiva, and iris showed no signs of damage or irritation (Fig. 7A) [22]. The scores for discharge and conjunctival damage were zero for all observations up to 8 h. The corneal opacity and hyperemia of the iris were graded as zero at all stages. These findings supported the use of TRM in nanoparticulate form for improved ocular retention.

3.9. Mucoadhesive evaluation

The mucoadhesive evaluations for the CS, TCS, and NT8 formulations are shown in Fig. 7B. The mucoadhesion time of the CS was 5.7 h and of the TCS was 7.6 h. This indicated that the thiolation of CS enhanced the time of mucoadhesion because of the presence of the thiol group in the TCS. The nanoparticles of NT8 had a 7.5 h mucoadhesion time because of the disulfide linkage between the TCS and the mucus of the eye [36]. The obtained *p*-value was 0.001 and for the mucoadhesion study, indicating that the results were statistically significant.

3.10. HPLC method development

HPLC method for TRM determination was established, followed by its validation. An optimal TRM detection time of 3.627 min was obtained as shown in Fig. 8. The linearity graph shows that the TRM has a good regression value of 0.9993. TRM was reported to have limits of detection (LOD) and quantitation (LOQ) of 4.57 μg/mL and 8.71 μg/mL, respectively. The developed method's high mean TRM recovery percentage (98.78%) revealed its great accuracy [41]. Inter-day and intra-day precision (% RSD) of TRM were calculated and found to be less than 2%.

3.11. In vivo retention and pharmacokinetics of TRM

In order to assess the potential of the TRM-loaded nanoparticles for prolonged residency at the cornea, the appropriate therapeutic

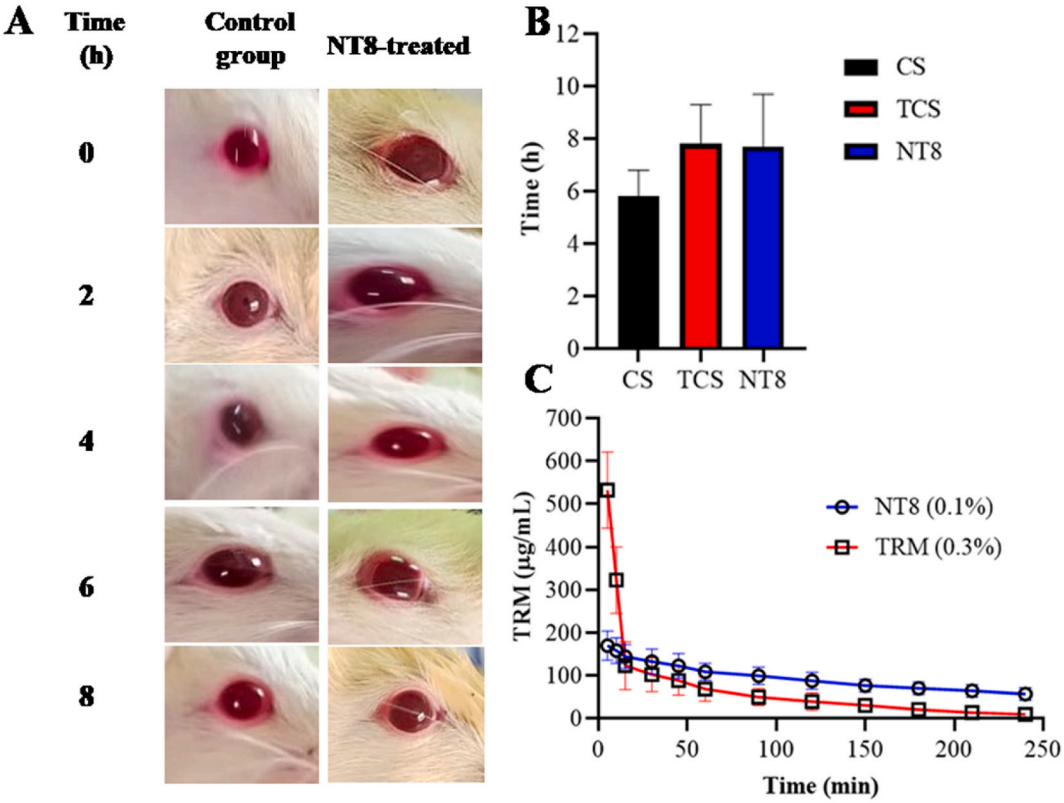

Fig. 7. Ocular irritation, mucoadhesion and pharmacokinetic analysis of developed nanoparticles. (A) Results of irritation of albino rat eyes lasting up to 8 h. (B) Adhesion of CS, TCS, and NT8 nanoparticles. (C) Peak plasma concentrations of TRM 0.3% and NT8 0.1% formulations. All signs such as discharge and conjunctival damage were absent in the eyes of albino rats during draize test.

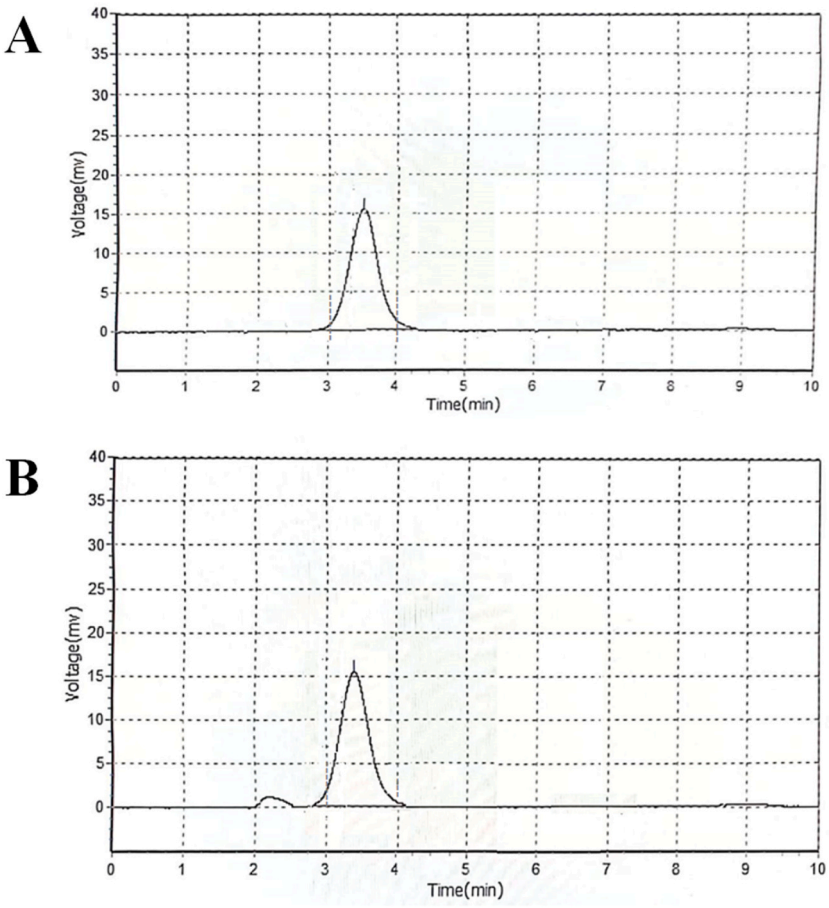

Fig. 8. Chromatograms of pure TRM (A) and drug loaded nanoparticles containing TRM (B).

concentration at the cornea with a small dose, and the increased antibacterial efficacy relative to TRM, pharmacokinetic tests were done. In sheep, the ocular pharmacokinetics of the NT8 0.1% (w/v) formulation and the TRM supplied as a commercial product (TRM 0.3% w/v) were compared (Table 5 and Fig. 7C). The dosage volume was the same for both formulations, but the strengths varied. This difference in dosage strength was chosen to assess the effectiveness of the nanoparticles and their capacity to lower doses [40]. Another goal was to reach the ideal C_{max}, which was not overly high relative to that of the TRM, to lessen TRM's naso-lacrimal elimination and prevent any negative effects from repeated administration. The NT8 formulation greatly increased the $AUC_{(0-\infty)}$ (1.5-fold) while significantly reducing the clearance (5-fold). The MRT of NT8 was noticeably higher than that of the TRM. As a result, the eye surface may have experienced a binding force from the positively charged nanoparticles. However, the positive charge was not the only factor that affected the bioadhesion of TCS. The presence of free -NH2 and –OH groups from TCS molecules, which form hydrogen bonds with the mucin on the surface of the eye, may have further encouraged it [42]. In pharmacokinetics, a *p*-value of less than 0.05 indicates that the results are statistically significant. According to the pharmacokinetic investigation, the newly developed formulation greatly improved the medication's absorption performance over the pure drug due to improved solubility properties.

4. Conclusions

Nanoparticles of TCS were successfully prepared using ionic gelation method. The mean diameter of prepared nanoparticles was in the range of 73–189 nm, a suitable size in ocular drug delivery that does not cause irritation. In the current work, we proved that the TCS nanoparticles loaded with TRM resulted in improved precorneal retention, sustained drug release, and high ocular availability at low doses and dosing frequencies. As a result of the interaction between the TCS and mucus, the nanoparticles of TCS might be thought of as increased mucoadhesive polymers. The TCS nanoparticles had both strong surface charge–dependent mucoadhesive characteristics and adequate entrapment efficiency. According to the findings of the *in vitro* release investigation, TRM was released from TCS nanoparticles over an extended period of time and in accordance with the fickian theory of diffusion. By reducing the frequency of delivery, the drug's relatively longer release increases patient compliance. The cornea, conjunctiva, and iris did not show any signs of a clinical abnormality or ocular injury. The study also provided information on the ocular pharmacokinetic profile of the TRM, which might be used to develop future dose regimens and formulations. Due to its capacity to maintain a consistent drug release and its

Table 5
Topical application and pharmacokinetic analysis of NT8 and TRM in the precorneal region of sheep (n = 3).

Parameter	Unit	NT8 (0.1%)	TRM (0.3%)	*p*-value
C_{max}	μg/mL	169.67 ± 6.09	532.45 ± 23.31	0.0012
$t_{1/2}$	min	50.04 ± 3.07	09.56 ± 1.34	<0.0001
$AUC_{(0-\infty)}$	min × μg/mL	12078.45 ± 87.34	8059.45 ± 67.31	0.0032
MRT	min	76.45 ± 3.45	13.21 ± 2.31	0.0023
Cl	mL/min	0.014 ± 0.0001	0.113 ± 0.002	0.0002

convenience of administration due to the lesser need for frequent dosages, this innovative formulation was an effective substitute for traditional ophthalmic suspensions. Beneficial characteristics of TCS nanoparticles improved retention of the delivery system in the eye. However, more research is needed to assess its clinical efficacy.

Limitations of the study

The reporting of long tern stability study is the major limitation of the research work.

Funding

This project was funded by the Deanship of Scientific Research (DSR) at King Abdulaziz University, Saudi Arabia, Jeddah, under grant no. (RG-2-166-43). The authors, therefore, acknowledge with thanks DSR for technical and financial support.

Author's contribution

Sadaf Javed and Ghulam Abbas- Conceived and designed the experiments and analyzed and interpreted the data. Shahid Shah, Akhtar Rasul, Muhammad Irfan and Ammara Saleem- Performed the experiments and wrote the paper. Khaled M. Hosny, Sahar M. Bukhary, Awaji Y. Safhi, Fahad Y. Sabei, Mohammed A. Majrashi, Hala M. Alkhalidi and Mohammed Alissa- Conceived and designed the experiments and Contributed reagents, materials, analysis tools or data; Sajid Mehmood Khan and Muhammad Hanif- Performed the experiments and wrote the paper.

Declaration of competing interest

The authors declare that they have no known competing financial interests or personal relationships that could have appeared to influence the work reported in this paper.

Acknowledgments

This project was funded by the Deanship of Scientific Research (DSR) at King Abdulaziz University, Jeddah, under grant no. (RG-2-166-43). The authors, therefore, acknowledge with thanks DSR for technical and financial support.

References

[1] C.S. De Paiva, A.J. Leger, R.R. Caspi, Mucosal immunology of the ocular surface, Mucosal Immunol. 15 (2022) 1143–1157.
[2] E. Delair, P. Latkany, A.G. Noble, P. Rabiah, R. McLeod, A. Brézin, Clinical manifestations of ocular toxoplasmosis, Ocul. Immunol. Inflamm. 19 (2011) 91–102.
[3] S.K. Linden, P. Sutton, N.G. Karlsson, V. Korolik, M.A. McGuckin, Mucins in the mucosal barrier to infection, Mucosal Immunol. 1 (2008) 183–197.
[4] K.G. Deepthi, S.R. Prabagaran, Ocular bacterial infections: pathogenesis and diagnosis, Microb. Pathog. 145 (2020), 104206;
(a) S.K. Sahoo, F. Dilnawaz, S. Krishnakumar, Nanotechnology in ocular drug delivery, Drug Discov. Today 13 (2008) 144–151.
[5] S.K. Sahoo, F. Dilnawaz, S. Krishnakumar, Nanotechnology in ocular drug delivery, Drug Discov. Today 13 (2008) 144–151.
[6] I.P. Kaur, A. Garg, A.K. Singla, D. Aggarwal, Vesicular systems in ocular drug delivery: an overview, Int. J. Pharm. 269 (2004) 1–4.
[7] N.K. Mehra, D. Cai, L. Kuo, T. Hein, S. Palakurthi, Safety and toxicity of nanomaterials for ocular drug delivery applications, Nanotoxicology 10 (2016) 836–860.
[8] A. Patel, K. Cholkar, V. Agrahari, A.K. Mitra, Ocular drug delivery systems: an overview, World J. Pharmacol. 2 (2013) 47–64.
[9] J.J. Wang, Z.W. Zeng, R.Z. Xiao, T. Xie, G.L. Zhou, X.R. Zhan, S.L. Wang, Recent advances of chitosan nanoparticles as drug carriers, Int. J. Nanomed. 6 (2011) 765–774.
[10] N. Omerović, E. Vranić, Application of nanoparticles in ocular drug delivery systems, Health Technol. 10 (2020) 61–78.
[11] M.A. Kalam, The potential application of hyaluronic acid coated chitosan nanoparticles in ocular delivery of dexamethasone, Int. J. Biol. Macromol. 89 (2016) 559–568.
[12] M.J. Mitchell, M.M. Billingsley, R.M. Haley, M.E. Wechsler, N.A. Peppas, R. Langer, Engineering precision nanoparticles for drug delivery, Nat. Rev. Drug Discov. 20 (2021) 101–124.
[13] V. Dodane, V.D. Vilivalam, Pharmaceutical applications of chitosan, Pharmaceut. Sci. Technol. Today 1 (1998) 246–253.
[14] A. Bernkop-Schnürch, M. Hornof, D. Guggi, Thiolatedchitosans, Eur. J. Pharm. Biopharm. 57 (2004) 9–17.
[15] R. Esquivel, J. Juárez, M. Almada, J. Ibarra, M.A. Valdez, Synthesis and characterization of new thiolated chitosan nanoparticles obtained by ionic gelation method, Int. J. Polym. Sci. 2015 (2015) 1–19.
[16] A.M. Dos Santos, S.G. Carvalho, L.M.B. Ferreira, M. Chorilli, M.P.D. Gremião, Understanding the role of electrostatic interactions on the association of 5-fluorouracil to chitosan-TPP nanoparticles, Colloids Surf. A Physicochem. Eng. Asp. 640 (2022), 128417.
[17] M.L. Bruschi, Strategies to Modify the Drug Release from Pharmaceutical Systems, Woodhead Publishing, 2015.

[18] R. Mohapatra, S. Senapati, C. Sahoo, S. Mallick, Transcorneal permeation of diclofenac as a function of temperature from film formulation in presence of triethanolamine and benzalkonium chloride, Colloids Surf. B Biointerfaces 123 (2014) 170–180.
[19] R. Bhatta, H. Chandasana, Y. Chhonker, C. Rathi, D. Kumar, K. Mitra, P. Shukla, Mucoadhesive nanoparticles for prolonged ocular delivery of natamycin: in vitro and pharmacokinetics studies, Int.J. Pharm. 432 (2012) 105–112.
[20] Y. Hilliam, S. Kaye, C. Winstanley, Pseudomonas aeruginosa and microbial keratitis, J. Med. Microbiol. 69 (2020) 3–13.
[21] A. Dave, A. Samarth, R. Karolia, S. Sharma, E. Karunakaran, L. Partridge, S. MacNeil, P.N. Monk, P. Garg, S. Roy, Characterization of ocular clinical isolates of Pseudomonas aeruginosa from non-contact lens related keratitis patients from South India, Microorganisms 8 (2020) 260.
[22] Z. Jafariazar, N. Jamalinia, F. Ghorbani-Bidkorbeh, S.A. Mortazavi, Design and evaluation of ocular controlled delivery system for diclofenac sodium, Iran. J. Pharm. Res. (IJPR) 14 (2015) 23–31.
[23] B. Akhtar, F. Muhammad, B. Aslam, M.K. Saleemi, A. Sharif, Pharmacokinetic profile of chitosan modified poly lactic co-glycolic acid biodegradable nanoparticles following oral delivery of gentamicin in rabbits, Int. J. Biolog. Macromol. 164 (2020) 1493–1500.
[24] S. Singh, P. Mishra, Bacitracin and isothiocyanate functionalized silver nanoparticles for synergistic and broad spectrum antibacterial and antibiofilm activity with selective toxicity to bacteria over mammalian cells, Mater. Sci. Eng. C (2022), 112649.
[25] L.M. Armijo, S.J. Wawrzyniec, M. Kopciuch, Y.I. Brandt, A.C. Rivera, N.J. Withers, N.C. Cook, D.L. Huber, T.C. Monson, H.D. Smyth, Antibacterial activity of iron oxide, iron nitride, and tobramycin conjugated nanoparticles against *Pseudomonas aeruginosa* biofilms, J. Nanobiotechnology 18 (2020) 1–27.
[26] N.K. Al-Nemrawi, N.A.H. Alshraiedeh, A.L. Zayed, B.M. Altaani, Low molecular weight chitosan-coated PLGA nanoparticles for pulmonary delivery of tobramycin for cystic fibrosis, Pharmaceuticals 11 (2018) 28.
[27] M.A. Rosasco, S.L. Bonafede, S.N. Faudone, A.I. Segall, Compatibility study of tobramycin and pharmaceutical excipients using differential scanning calorimetry, FTIR, DRX, and HPLC, J. Therm. Anal. Calorim. 134 (2018) 1929–1941.
[28] I. Ali, C. Peng, T. Ye, I. Naz, Sorption of cationic malachite green dye on phytogenic magnetic nanoparticles functionalized by 3-mercaptopropionic acid, RSC Adv. 8 (2018) 8878–8897.
[29] S. Patere, B. Newman, Y. Wang, S. Choi, S. Vora, A.W. Ma, M. Jay, X. Lu, Influence of manufacturing process variables on the properties of ophthalmic ointments of tobramycin, Pharm. Res. (N. Y.) 35 (2018) 1–16.
[30] M.L. Del Prado-Audelo, I.H. Caballero-Florán, J. Sharifi-Rad, N. Mendoza-Muñoz, M. González-Torres, Z. Urbán-Morlán, B. Florán, H. Cortes, G. Leyva-Gómez, Chitosan-decorated nanoparticles for drug delivery, J. Drug Deliv. Sci. Technol. 59 (2020), 101896.
[31] M.T. Pelegrino, J.C. Pieretti, G. Nakazato, M.C. Gonçalves, J.C. Moreira, A.B. Seabra, Chitosan chemically modified to deliver nitric oxide with high antibacterial activity, Nitric Oxide 106 (2021) 24–34.
[32] V. Sharma, P. Ilaiyaraja, A.C. Dakshinamurthy, C. Sudakar, One step thermolysis of Sb-Mercaptopropionic acid complex in ambient air atmosphere for growing Sb2S3 thin films with controlled microstructure, Mater. Sci. Semicon. Process 121 (2021), 105330.
[33] P. Ilaiyaraja, V. Sharma, A.C. Dakshinamurthy, T.K. Das, C. Sudakar, Fabrication of metal chalcogenide thin films by a facile thermolysis process under air ambient using metal-3-mercaptopropionic acid complex, Mater. Res. Bull. 141 (2021), 111346.
[34] A. Kaur, P. Kumar, L. Kaur, R. Sharma, P. Kush, Thiolated chitosan nanoparticles for augmented oral bioavailability of gemcitabine: preparation, optimization, in vitro and in vivo study, J. Drug Deliv. Sci. Technol. 61 (2021), 102169.
[35] A. Anitha, N. Deepa, K. Chennazhi, S. Nair, H. Tamura, R. Jayakumar, Development of mucoadhesive thiolated chitosan nanoparticles for biomedical applications, Carbohydr. Polym. 83 (2011) 66–73.
[36] M.S. Kazemi, Z. Mohammadi, M. Amini, M. Yousefi, P. Tarighi, S. Eftekhari, M.R. Tehrani, Thiolated chitosan-lauric acid as a new chitosan derivative: synthesis, characterization and cytotoxicity, Int. J. Biolog. Macromol. 136 (2019) 823–830.
[37] P. Mura, F. Maestrelli, M. Cirri, N. Mennini, Multiple roles of chitosan in mucosal drug delivery: an updated review, Mar. Drugs 20 (2022) 335.
[38] N.K. Al-Nemrawi, R.Q. Alkhatib, H. Ayyad, A. Nid''A, Formulation and characterization of tobramycin-chitosan nanoparticles coated with zinc oxide nanoparticles, Saudi Pharm. J 30 (2022) 454–461.
[39] R. Ferraz, D. Silva, A.R. Dias, V. Dias, M.M. Santos, L. Pinheiro, C. Prudêncio, J.P. Noronha, Ž. Petrovski, L.C. Branco, Synthesis and antibacterial activity of ionic liquids and organic salts based on penicillinG and amoxicillin hydrolysate derivatives against resistant bacteria, Pharmaceutics 12 (2020) 221.
[40] G. Abbas, A. Rasul, M. Fakhar-e-Alam, M. Saadullah, S. Muzammil, O. Iqbal, M. Atif, M. Hanif, S. Shah, S. Ahmad, Nanoparticles of thiolated chitosan for controlled delivery of moxifloxacin: in-vitro and in-vivo evaluation, J. King Saud Univ. Sci. 34 (2022), 102218.
[41] M. Mashat, H. Chrystyn, B.J. Clark, K.H. Assi, Development and validation of HPLC method for the determination of tobramycin in urine samples post-inhalation using pre-column derivatisation with fluorescein isothiocyanate, J. Chromatogr. B 869 (2008) 59–66.
[42] B.B. Dias, F. Carreño, V.E. Helfer, P.M.B. Garzella, D.M.F. de Lima, F. Barreto, de Araújo, B. V, T. Dalla Costa, Probability of target attainment of tobramycin treatment in acute and chronic *Pseudomonas aeruginosa* lung infection based on preclinical population pharmacokinetic modeling, Pharmaceutics 14 (2022) 1237.